ACS APPLIED BIO MATERIALS

www.acsabm.org

Article

Physicochemical Characterization, Stability, and In Vitro Evaluation of Curcumin-Loaded Solid Lipid Nanoparticles Prepared Using Biocompatible Synthetic Lipids

Swagata Patra, Joykrishna Dey,* and Avik Chakraborty

Cite This: *ACS Appl. Bio Mater.* 2023, 6, 2785−2794

Read Online

ACCESS | Metrics & More | Article Recommendations | Supporting Information

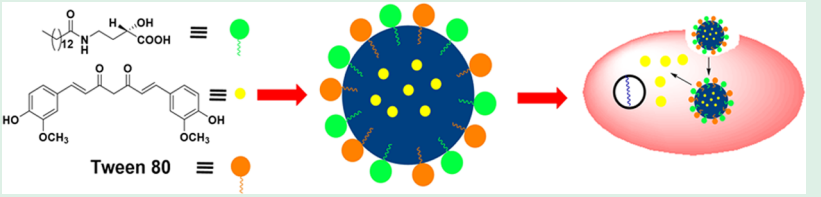

ABSTRACT: Solid lipid nanoparticles (SLNs) are promising drug delivery vehicles for the delivery of various drugs, especially poorly water-soluble drugs. However, the aqueous stability, drug release, and biocompatibility of SLNs are some of the issues that need attention. In this work, curcumin-loaded SLNs were prepared, and morphology, particle size, and entrapment efficiency were studied. For this, two amino acid-derived lipids were developed. The effect of the polarity of the lipid head on the aqueous stability of the SLN dispersion was investigated. Based on the stability, particle size, and polydispersity, an optimum formulation was obtained. The curcumin entrapment efficiency of the SLNs was found to be greater than those reported in the literature. The entrapped curcumin, as well as curcumin-loaded SLN suspensions, exhibited improved storage stability. The in vitro release kinetics indicated an enhanced rate of drug release in the case of curcumin-loaded SLNs consisting of the lipid containing −OH groups at the lipid head. The pure lipid and the blank SLN were found to have no significant cytotoxicity, but curcumin and curcumin-loaded SLNs induced cell death in a concentration-dependent manner in both human prostatic adenocarcinoma PC3 cell line and human breast carcinoma MCF7 cell line. This study has proposed a potential semisynthetic lipid for the stable SLN suspension for the delivery of curcumin.

KEYWORDS: *SLN, curcumin, calorimetry, microscopy, cytotoxicity*

INTRODUCTION

Curcumin (CUR; Figure 1) has been widely used in medicine due to its antibacterial, anti-inflammatory, antioxidant, and antitumor effects.[1,2] In recent literature, CUR has been shown to have anticancer properties against breast, ovarian, neurological, and lung cancer.[3−6] However, delivery of CUR is limited by its poor aqueous solubility, chemical stability, and hence poor bioavailability. Therefore, new strategies are required to improve the therapeutic efficacy of such hydrophobic drugs. The solubility and stability issues can be resolved by encapsulating it into nanoaggregates that enhance its aqueous solubility and protect it from degradation and metabolism. Extensive research has been carried out in the past to develop various nanoformulations of anticancer drugs. Different nanocarriers, such as polymer nanoparticles (PNs),[7] polymeric micelles (PMs),[8] liposomes,[9] nanoemulsions (NEs),[10] nanogels,[11] solid lipid nanoparticles (SLNs),[12] polymer conjugates,[13] have been investigated for the delivery of anticancer drugs to tumor cells. Recently, CUR-loaded SLNs were also found to show improved therapeutic efficacy for breast cancer.[14]

Thus, SLNs have emerged as a promising drug delivery system specifically for drugs of poor aqueous solubility.[15−22] SLNs have received massive attention because of their potential application in targeted drug delivery. SLNs usually consist of biocompatible lipids, such as fatty acids; mono-, di-, and triglycerides; and so on. The hydrophobic lipid core of SLN provides a perfect environment for the entrapment of various hydrophobic drugs, while the hydrophilic head group helps enhance its bioavailability and biocompatibility. In the last two decades, a number of commercially available lipids, such as stearic acid, palmitic acid, glyceryl mono- and di-stearate, etc., have been employed for SLN preparation.[23−30] The choice of lipid, however, is very important in SLN-based nanoformulations. SLNs prepared using commercially available lipids were observed to suffer from limited storage stability, low encapsulation efficiency, and poor release kinetics. As SLN formulations tend to form an insoluble

Received: April 4, 2023
Accepted: June 21, 2023
Published: July 5, 2023

https://doi.org/10.1021/acsabm.3c00252
ACS Appl. Bio Mater. 2023, 6, 2785−2794

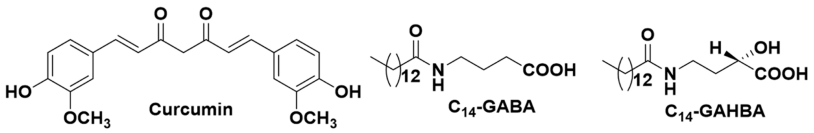

Figure 1. Chemical structure of curcumin, C_{14}-GABA, and C_{14}-GAHBA.

precipitate in physiological conditions, their colloidal stability needs to be improved before any preclinical development. Synthetic lipid molecules, however, can offer numerous advantages. For example, the chain length of the lipid can be varied to accommodate a variety of drugs with wide molecular weight and size ranges. The head group of the lipid molecule can be modified to increase colloidal stability and bioavailability and to lower the cytotoxicity. Most importantly, synthetic lipids can be modified with a target-specific agent to increase the specificity of the SLN toward a particular disease site.

The SLN can play an important role in delivering CUR into disease sites with enhanced bioavailability and improved overall effects. The present study is primarily aimed at developing CUR-loaded SLNs with enhanced storage stability. Therefore, in this study, we have designed and developed two lipids 4-*N*-(*n*-tetradecanoylamino)butyric acid (C_{14}-GABA) and 4-*N*-(*n*-tetradecanoylamino)-2-hydroxybutyric acid (C_{14}-GAHBA) (see Figure 1 for structures) for the preparation of CUR-loaded SLNs. In designing C_{14}-GABA, two biocompatible molecules, such as myristic acid and γ-aminobutyric acid (GABA), were conjugated via a hydrolyzable amide linkage. In the same way, S-(−)-γ-amino-2-hydroxybutyric acid (GAHBA) and myristic acid were conjugated to obtain C_{14}-GAHBA. GABA is a nonprotein amino acid and is found in bacteria, plants, and vertebrates.[31,32] GABA was found to be a chief inhibitory neurotransmitter in the central nervous system. The chemical, physiological, and pharmacological roles of GABA have been reviewed in the literature.[33,34] The incorporation of biomolecules like fatty acids and GABA is expected to make C_{14}-GABA (or C_{14}-GAHBA) cells viable. Also, the chiral head group of C_{14}-GAHBA can enhance the interaction of the SLN with chiral molecules. Thus, the modification of the −COOH group of the fatty acid with a γ-amino acid is expected to enhance the biocompatibility and bioavailability of the SLN. Further, the presence of −CONH−, −OH, and free −COOH groups in the structure of the lipid will enhance the storage stability of the SLN suspension. Further, the C_{14}-GAHBA lipid is also expected to increase the degradation rate by allowing the water molecules to penetrate easily into the pores of the matrix, leading to enhanced drug release. In order to demonstrate improved entrapment efficiencies and release profiles of the C_{14}-GABA- and C_{14}-GAHBA-based SLNs, CUR-loaded SLNs (CUR-SLNs) were prepared and characterized. The physical and chemical stability of the SLN formulations was investigated. The in vitro release kinetics of CUR were also studied. The in vitro cytotoxicity of free CUR and CUR-SLNs against human breast cancer cells (MCF7) and human prostatic adenocarcinoma cells (PC3) was investigated.

EXPERIMENTAL SECTION

Materials. S-(−)-γ-amino-α-hydroxybutyric acid (GAHBA), γ-aminobutyric acid (GABA), *n*-tetradecanoyl chloride, egg-lecithin (EL), curcumin (CUR), and poly(vinyl alcohol) (PVA, MW = 14 kDa) were purchased from Sigma-Aldrich (Bangalore, India). Tween 40 (T40), Tween 60 (T60), and Tween 80 (T80) were obtained from Alfa Aesar (Kolkata, India). Tetrahydrofuran (THF) was purchased from Merck (Mumbai, India). Analytical-grade hydrochloric acid and triethylamine (TEA) were procured from SRL (Mumbai, India). Dimethyl sulfoxide (DMSO-d_6) and chloroform-*d* ($CDCl_3$) were purchased from Cambridge Isotope Laboratory. Ethanol (EtOH), methanol, THF, and TEA were dried and freshly distilled before use. For the preparation of aqueous solutions, Milli-Q water (resistivity >18.2 MΩ cm) was used.

Lipids C_{14}-GABA and C_{14}-GAHBA were synthesized and purified according to the reported procedure, the details of which are available in the Supporting Information (SI). FTIR, ^{1}H NMR, ^{13}C NMR, and HRMS spectra (see Figures S1−S4), which can be found in the SI, were used to determine the chemical structure of the lipids.

General Instrumentation. An InstInd (Kolkata, India) melting point apparatus was used for melting point measurements. The pH measurements were performed on a digital pH meter (Model 111, India). Deionized water was obtained from a Milli-Q water purification system (IQ 7000, Merck Life Science Private Limited, Bengaluru, India). A PerkinElmer RX1 FTIR spectrometer was used for recording FTIR spectra. A Shimadzu UV-2450 (Japan) spectrophotometer was used for the measurements of UV−vis spectra. The measurements of ^{1}H and ^{13}C NMR spectra were performed on an AVANCE DAX-500 (Bruker, Sweden) 500 MHz NMR spectrometer. HRMS spectra were recorded on a 6545XT AdvanceBio LC/Q-TOF system (Agilent Technologies, Germany). Fluorescence emission spectra of CUR were recorded at an excitation wavelength (λ_{ex}) of 425 nm on a Hitachi F-7000 (Japan) spectrofluorometer.

Dynamic Light Scattering and ζ-Potential Measurements. A Zetasizer (Nano ZS 90, Malvern Instruments, Malvern, U.K.) dynamic light scattering (DLS) spectrometer was used to measure the mean particle size (*z*-average) and polydispersity index (PDI). The ζ-potential of the SLN dispersion was also measured by determining the particle electrophoretic mobility using the same DLS system. The SLN formulation was suitably diluted with Milli-Q (IQ 7000, Merck Life Science Private Limited, India) water to weaken opalescence before the measurement. The dilute SLN dispersion was further filtered through a 0.22 μm cellulose membrane filter.

Microscopy. Atomic force microscopy (AFM) measurements were performed a Nanoscope IIIA (Digital Instruments) in tapping mode under ambient conditions. For the sample preparation, a diluted 5 μL sample was placed on a glass slide and allowed to dry.

The morphology and shape of the blank and CUR-loaded SLNs were investigated by a transmission electron microscope (TEM) (TecnaiG^2 20 S-Twin, FEI, Netherlands). A diluted 4 μL SLN dispersion was drop-cast on a 400-mesh carbon-coated copper grid and allowed to stand for 1 min. The excess solution was carefully blotted off with tissue paper and allowed to dry overnight in vacuum desiccators before measurements.

Differential Scanning Calorimetry (DSC). A calorimeter DSC Q200 (PerkinElmer Instruments) was used for the measurements. Blank SLN or CUR-SLN powder was accurately weighed into aluminum pans, hermetically sealed, and measured against an empty reference pan. The pan was heated, and the thermogram was recorded in the temperature range of 50−200 °C at a heating rate of 10 °C/min.

SLN Preparation. SLNs were prepared using C_{14}-GABA and C_{14}-GAHBA as solid lipids by hot homogenization and ultrasonication methods.[35] Solid lipid (100 mg) and CUR (5−20 mg) mixtures were allowed to melt and mix in a hot water bath maintained at 85−90 °C. A pure surfactant or surfactant mixture was dissolved in Milli-Q water and heated to 85−90 °C in a water bath while stirring. The hot surfactant solution (10 mL) was poured slowly into the lipid melt and stirred at 800 rpm for 5 min using a magnetic stirrer while maintaining the temperature at around 85−90 °C. The hot o/w emulsion was then

https://doi.org/10.1021/acsabm.3c00252
ACS Appl. Bio Mater. 2023, 6, 2785−2794

Table 1. Mean Hydrodynamic Diameter (d_h), Polydispersity Index (PDI), ζ-Potential (ZP), and Storage Stability of Nanodispersions Containing 0.5% (w/v) C_{14}-GABA or C_{14}-GAHBA Lipids in the Presence of T80, T60, T40, EL, and PVA

surfactant (% w/v)								
T80	T60	T40	EL	PVA	d_h (nm)	PDI	ZP (mV)	storage stability
2.5					130 ± 5	0.226	−29 ± 4	45 days
	2.5				470 ± 30			precipitation observed after 1 day
		2.5			560 ± 140			precipitation observed after 1 day
2.0			0.5		44 ± 7	0.317	−36 ± 5	precipitated after 3 days
2.0				0.5	154 ± 9	0.313	−19 ± 2	stable for up to 15 days
1.0					>2000			precipitation observed after 2 days
1.5					620 ± 50			precipitation observed after 3 days
2.0					235 ± 5	0.479	−18 ± 2	precipitation observed after 5−6 days
[a]2.5					200 ± 5	0.484	−21± 3	precipitation observed after 2−3 days

[a]Prepared using C_{14}-GABA lipids.

Table 2. Mean Hydrodynamic Diameter (d_h), Polydispersity Index (PDI), ζ-Potential (ZP), and Encapsulation Efficiency (EE %) of CUR-SLN Formulations Prepared Using Varying CUR/lipid Ratios at Room Temperature (~25 °C)

formulation code	CUR/lipid (w/w)	d_h (nm)	PDI	ZP (mV)	EE(%) (±8)
SLN1	0.000	130 ± 5	0.226 ± 0.054	−29 ± 4	
[a]SLN2	0.000	200 ± 5	0.484 ± 0.018	−21± 3	
CUR-SLN1	0.050	142 ± 20	0.195 ± 0.017	−31 ± 2	96
CUR-SLN2	0.067	200 ± 30	0.342 ± 0.058	−26 ± 5	86
CUR-SLN3	0.100	233 ± 62	0.432 ± 0.096	−30 ± 2	98
[a]CUR-SLN4	0.100	225 ± 25	0.586 ± 0.086	−19 ± 5	90

[a]Prepared using C_{14}-GABA lipids.

sonicated for 10 min by use of a probe sonicator (Oscar Ultrasonics, Mumbai, India) to reduce the size of primary oil droplets. The hot nanoemulsion thus obtained was immediately dispersed in an equal volume (10 mL) of ice-cold water (or aqueous PVA solution) and stirred at 1200 rpm for 10 min using a magnetic stirrer. The same procedure was followed for the preparation of blank SLN without CUR. The CUR-to-lipid ratio was varied to prepare SLNs of different compositions. The details of the formulations are provided in Tables 1 and 2.

Determination of Encapsulation Efficiency. The encapsulation efficiency (EE) of SLN formulations was estimated spectrophotometrically by measuring the absorbance of CUR at a wavelength of 425 nm using a UV−vis spectrophotometer (Shimadzu UV-2450, Japan). The amount of unencapsulated drug in the SLN was removed by centrifugation at 8900 rpm for 60 min at 4 °C. Then, the samples were diluted in methanol, and absorbance was recorded. The EE was calculated using the following formula

$$\mathrm{EE}(\%) = (w_e/w_i) \times 100 \quad (1)$$

where w_i indicates the initial weight of the drug and w_e indicates the amount of drug entrapped in the nanoparticles.

In Vitro Drug Release Kinetics. An in vitro drug release study was performed using the dialysis method. The dialysis bag (Mw cutoff 14 kDa) was soaked in deionized water for 24 h before use. A 2 mL volume of CUR-SLN suspension was added to a dialysis bag. The sealed bag was placed in a beaker containing 50 mL of phosphate buffer pH 7.4 containing 2.5% T80 maintained at 37 °C. A 3 mL volume of the dissolution media was removed at regular intervals and replaced with the same volume of fresh medium to maintain the condition of the release medium. The samples were appropriately diluted, and the amount of CUR released was measured by spectrophotometric analysis.

In Vitro Cytotoxicity Assay. An in vitro cell cytotoxicity study of CUR-SLN was performed using human prostatic adenocarcinoma cell line PC3 (ATCC, CRL-1435) and human breast carcinoma cell line MCF7 (ATCC HBT-22) using the methodology described earlier.[36] The cell lines were obtained from Cell Repository, NCCS, Pune. Cells were grown in Iscove's modified Dulbecco's medium (IMDM) supplemented with 10% FBS, 1% L-glutamate, and 80 μg/mL gentamycin sulfate. Cells were maintained and cultured in 25 cm^2 flasks and incubated in 5% CO_2 in humidified air at 37 °C.

The cytotoxic potential of CUR-SLNs was assessed using MTT reduction[37] in PC3 and MCF7 cell lines. Briefly, 1×10^4 cells per well were seeded in 96-well plates and incubated overnight. Twelve hours later, cells were treated with CUR (5−40 μg/mL), CUR-SLN (5−40 μg/mL), or blank SLN for 24 h. As CUR was dissolved in DMSO, the highest effective concentration of DMSO in the treatment groups was used as the vehicle control. Cells were washed with PBS and incubated further for 3 h with 100 μL of 0.5 mg/mL MTT. The formazan crystals formed were dissolved in 100 μL of 10% SDS for 2 h, and absorbance was measured at 570 nm using a microplate spectrophotometer (iMax, BioRad). Each treatment was carried out in triplicate, with each experiment being repeated at least twice. For the MTT assay, the relative cell viability (%) compared to the control cells was calculated using the following equation

$$\text{cell viability}(\%\ \text{of the sample}) = (A_{\text{sample}}/A_{\text{control}}) \times 100 \quad (2)$$

where A_{sample} and A_{control} are the absorbance values obtained for cells treated with SLN and for cells incubated with the culture medium, respectively. A histogram of different drug formulations versus percent cell viability was plotted.

Software and Statistical Data Analysis. All statistical analyses and plotting were performed by OriginPro8 software. NMR spectra were analyzed by MestReNova v7.1.0-9185 software (Mestrelab Research S.L). ChemDraw Ultra v12.0.2.1076 software (Cambridgesoft, PerkinElmer Informatics) was used as a drawing tool for chemical structures and reaction schemes. Measurements were done in triplicates to check the reproducibility of the results. Average values and standard deviations (SDs) were calculated, and the results were represented as mean ± SD, wherever possible.

RESULTS AND DISCUSSION

Selection of Lipids and Surfactants. For SLN-based formulations, the materials should be pharmaceutically acceptable, nonirritant, and generally regarded as safe (GRAS). Also, for SLN formulations, a higher solubility of the drug in the lipid

https://doi.org/10.1021/acsabm.3c00252
ACS Appl. Bio Mater. 2023, 6, 2785−2794

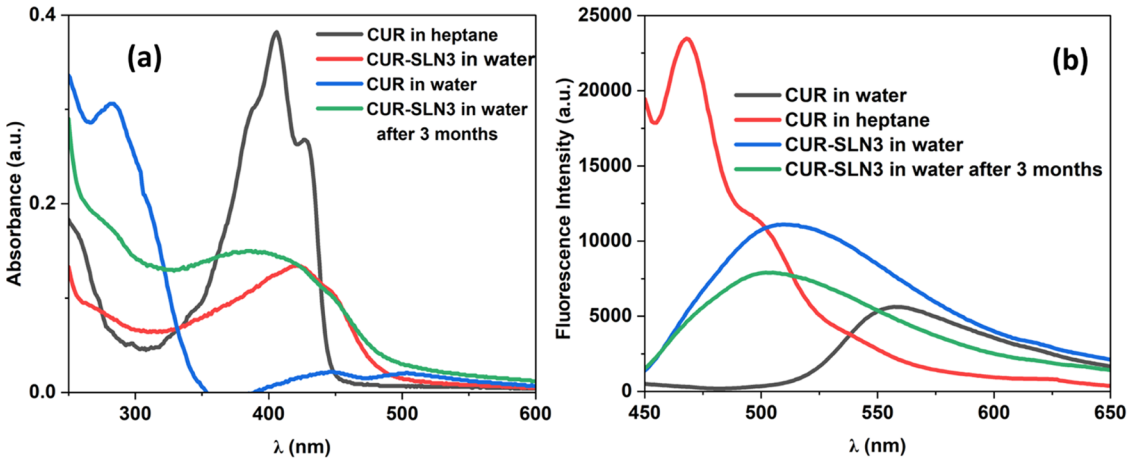

Figure 2. (a) UV−vis and (b) fluorescence spectra of CUR in heptane and water solvents, aqueous CUR-SLN3 suspension, and aqueous CUR-SLN3 suspension after 3 months.

is required so that the drug remains in the solubilized form. For solubility determination, a fixed amount (0.1 g) of the solid lipid was taken in different clear glass vials. Each vial was heated up to 90 °C to melt the lipid, and then solid CUR was added to each vial in increments of 3 mg until the disappearance of CUR in the melted lipid was observed. Thus, the solubility of CUR in the C_{14}-GAHBA melt was found to be about 10.7% (w/w), which is either greater than or comparable to its solubility in other lipids.[38]

Further, for a stable formulation, an optimum combination of surfactants with low and high hydrophilic−lipophilic balance (HLB) is required. The results of preliminary stability studies using T40, T60, T80, and EL surfactants are summarized in Table 1. It is observed that in the presence of the same amount (2.5%, w/v) of T80, T60, or T40, the surfactant size and PDI increased in order T80 < T60 < T40, and consequently, the particles were found to be least stable when T40 was used, which may be attributed to its shorter PEG chain length. T80 results in steric stabilization of the SLN due to the interpenetration of long PEG chains. This limits the freedom of the particles and prevents them from associating with one another. However, the use of EL, keeping the total amount of the surfactant constant, resulted in the precipitation of the lipid on storage in less than 3 days. Despite smaller particle sizes, the lowest storage stability of the SLN suspension was due to the formation of large mixed aggregates by the T80 and EL molecules. On the other hand, the use of the same weight percentage of PVA as a viscosity modifier increased the stability of the SLN suspension to 15 days despite a slight increase in the size of nanoparticles. As the SLN suspension was found to be most stable (45 days) in the presence of only T80 (HLB 15), it was selected as the surfactant for the SLN formulation.

SLN Formulation and Optimization. After the selection of the lipid and the surfactant, the composition of the formulation was optimized by selecting different proportions of the lipid and T80 surfactant in the formulations and visual observation of the physical stability. The reduction of surface tension by increasing surfactant concentration facilitates particle partition during homogenization and contributes to a reduction of particle size.[39] At lower surfactant concentrations, the SLN suspension was observed to have lower storage stability (Table 1). In the presence of 2.5% (w/v) T80, the SLN suspension was found to exhibit the highest stability (>1 month). Thus, the optimum T80 concentration was found to be 2.5%. It should be noted here that free −COOH and −OH groups present at the lipid head also provide extra stability to the SLN suspension by hydrogen bonding with water molecules in comparison to natural fatty acids of comparable chain lengths. The effect of −OH groups at the lipid head is also manifested by the higher stability of SLNs constituted by the C_{14}-GAHBA lipid in comparison to SLNs made using C_{14}-GABA (see Table 1).

In order to ensure an optimum EE value, the CUR-to-lipid ratio was varied. The SLN formulations thus prepared were left at room temperature and at 4 °C for visual observation from time to time. The formulations that did not exhibit the presence of any unentrapped CUR or precipitation of the lipid were considered to be stable. The relevant data are included in Table 2. As observed, the EE increases with the CUR-to-lipid ratio reaching a maximum at 1:10 (w/w). The size of the SLN is also observed to increase with an increase of CUR content, which led to the decrease of storage stability of the CUR-SLN. The data suggest that the combined method of hot homogenization and ultrasonication is suitable for SLN preparation.

Drug Encapsulation. The synthesized lipid molecule is biocompatible and biodegradable, and it has a suitable hydrophobic core that provides an appropriate environment for the entrapment of hydrophobic drugs in its core. In fact, the lipophilic or hydrophilic nature of the bioactive material is an important factor in achieving high encapsulation efficiency. Thus, for drugs like CUR that have higher hydrophobicity and hence have limited use in the clinical field, the SLN can play an important role in delivering these hydrophobic drugs into disease sites with enhanced bioavailability and improved overall effects. In this study, due to the lipophilic nature of CUR, an average EE of up to 98% was achieved (Table 2). This is higher in comparison to that of CUR-SLN reported in the literature.[38] The higher %EE can be associated not only with the long hydrocarbon chain length but also with the presence of −OH groups in the lipid structure. This is shown by the lower %EE of CUR-SLN4, for which a nonhydroxyl lipid C_{14}-GABA was used.

Drug−Lipid Interaction Studies. Due to the hydrophobic interaction, CUR is expected to be encapsulated within the hydrocarbon core of the SLNs. The CUR−lipid interaction was investigated using FTIR, UV−vis, and fluorescence spectroscopy by comparing respective spectral changes. The FTIR spectra of CUR, SLN1, and CUR-SLN3 are depicted in Figure S5. As can be seen, the FTIR spectra of SLN1 and CUR-SLN3 are very similar. In the FTIR spectrum of CUR-SLN3, the major

https://doi.org/10.1021/acsabm.3c00252
ACS Appl. Bio Mater. 2023, 6, 2785−2794

characteristic bands (ν(O−H), 3505 cm^{-1}; ν(C═C), 1627 cm^{-1}) corresponding to CUR disappeared. This is an indirect confirmation of CUR encapsulation within solid lipid nanoparticles with a weak or no interaction between CUR and lipid molecules in the SLN. This is also indicated by the UV−vis spectra (Figure 2a) of free CUR in the *n*-heptane solvent and CUR-SLN3 suspension in water. It can be seen that both spectra appear at an almost similar position. A small broadening of the CUR-SLN3 spectrum might be due to the different microenvironments of CUR molecules within the SLN matrix. Since the fluorescence spectrum is known to be more sensitive to changes in the environment,[40] we also measured the fluorescence spectra (Figure 2b) of the aqueous suspension of CUR-SLN3 and those of free CUR in *n*-heptane and water solvents, respectively. As in the UV−vis spectrum, structured emission bands are also observed in the fluorescence spectrum of CUR in *n*-heptane. However, the emission spectra of free CUR and CUR-SLN3 in water are broad and red-shifted relative to those of free CUR in the *n*-heptane solvent. The broadness of the spectrum clearly suggests that CUR molecules are not only solubilized within the hydrocarbon core of the SLN but are also entrapped near the surface of the SLN, where CUR molecules can interact with water. The emission spectrum of CUR-SLN3 is, however, blue-shifted relative to the fluorescence spectrum of free CUR in water. This is because the phenolic −OH groups of CUR can undergo excited-state ionization in an aqueous environment, giving rise to the formation of mono- and/or dianion species.[41] This clearly establishes the fact that CUR molecules are also solubilized near the surface of the SLN structure. However, active CUR is protected by the lipid matrix and cannot be liberated unless the SLN undergoes erosion in the physiological system.

State of Lipid Nanoparticles. For their use as drug delivery systems, the lipid molecules in SLN should be in a solid state. In order to verify this and determine the degree of lipid crystallinity in the SLN, we performed a DSC analysis of the lipid, CUR, and CUR-SLN3. The DSC thermograms are depicted in Figure 3,

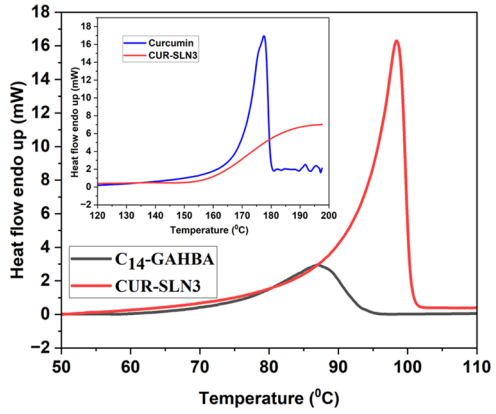

Figure 3. DSC thermograms of the C_{14}-GAHBA lipid and CUR-SLN3; inset, DSC thermograms of CUR and CUR-SLN3.

and relevant data are included in Table 3. The DSC thermogram of the C_{14}-GAHBA lipid containing a 14C chain exhibits a relatively broad endotherm peak (86.94 °C) with an onset at 74.84 °C, indicating melting of the amorphous lipid. The difference between onset and melting points can be taken as a measure of the peak width. The DSC thermogram of pure CUR, however, shows a sharp peak (177.5 °C) with the onset at 170.4 °C. The melting point was observed to be slightly higher than the reported melting point (173.1 °C), probably due to the existence of both keto and enol forms. In contrast to pure lipids, the thermogram of CUR-SLN3 shows a sharp endothermic peak at 98.4 °C with the onset at 93 °C, confirming the melting of the solid SLN. In fact, this is important for storage stability and sustained drug release. Also, it is interesting to note that the melting peak of CUR is not observed in the thermogram of CUR-SLN3, which confirms its entrapment within the solid lipid matrix of SLN. Also, it should be noted that the melting point of the lipid in the CUR-SLN3 system is slightly higher, which is opposite to what is expected for a colloidal system.[42] The more significant enthalpy change in CUR-SLN3 relative to the bulk lipid suggests a higher degree of lipid crystallinity in the SLN. In other words, the lipid molecules exist in a more ordered state in the SLN.

Table 3. Melting Parameters of CUR, C_{14}-GAHBA, and CUR-SLN3

sample	melting point (°C)	onset (°C)	peak width (°C)	enthalpy (J/g)
C_{14}-GAHBA	86.94	74.84	12.10	69.971
CUR	177.5	170.4	7.10	107.52
CUR-SLN3	98.39	92.85	5.54	107.01

Size and Morphology of SLN. The histograms of hydrodynamic size distribution are depicted in Figure 4, and the hydrodynamic diameter (d_h) and polydispersity index (PDI) data are summarized in Table 1. According to the data in Table 1, the mean d_h value of the SLN decreases with increasing T80 concentration. This is because of the reduction of surface tension with increasing surfactant concentration that facilitates particle partition during homogenization, leading to a reduction of particle size. In the presence of 2.5% (w/v) T80, the size of SLN was found to be the lowest. In fact, it has been reported that the use of T80 results in stable emulsions and finer-sized SLNs. At lower surfactant concentrations, the particle size is observed to be higher. This is due to the higher melting point of the lipid, which leads to less effective homogenization, resulting in bigger particle sizes and wider size distributions. The data in Table 2 suggest that the hydrodynamic diameter of the nanoparticles increases with increasing CUR concentration. This can be attributed to the higher encapsulation efficiency, which leads to an increase in size. The enlargement of SLN upon drug encapsulation is also shown by the higher d_h value of CUR-SLN4 in comparison to that of the corresponding blank SLN (SLN2).

The morphology of the SLN formulations was investigated by recording the TEM and AFM images of both blank and CUR-SLNs. The results are presented in Figure 5. The TEM pictures in Figure 5a, b confirm that the blank and drug-loaded SLNs are almost spherical in shape. Also, the size of blank SLN1 (90−100 nm) and CUR-SLN (80 nm) within the experimental error limit is closely similar. A similar observation can also be made from the AFM images in Figure 5c, d. The size of blank (43−61 nm) and CUR-loaded (40−50 nm) SLNs is slightly smaller than the corresponding value obtained from TEM pictures. However, the particle size obtained from TEM and AFM measurements is smaller than the corresponding value obtained from DLS measurements, which gives the size of hydrated particles. In contrast to DLS measurements, the TEM and AFM measurements require drying of the sample for the preparation of the specimen. Consequently, the micrographs of dried specimens exhibit smaller particles.

https://doi.org/10.1021/acsabm.3c00252
ACS Appl. Bio Mater. 2023, 6, 2785−2794

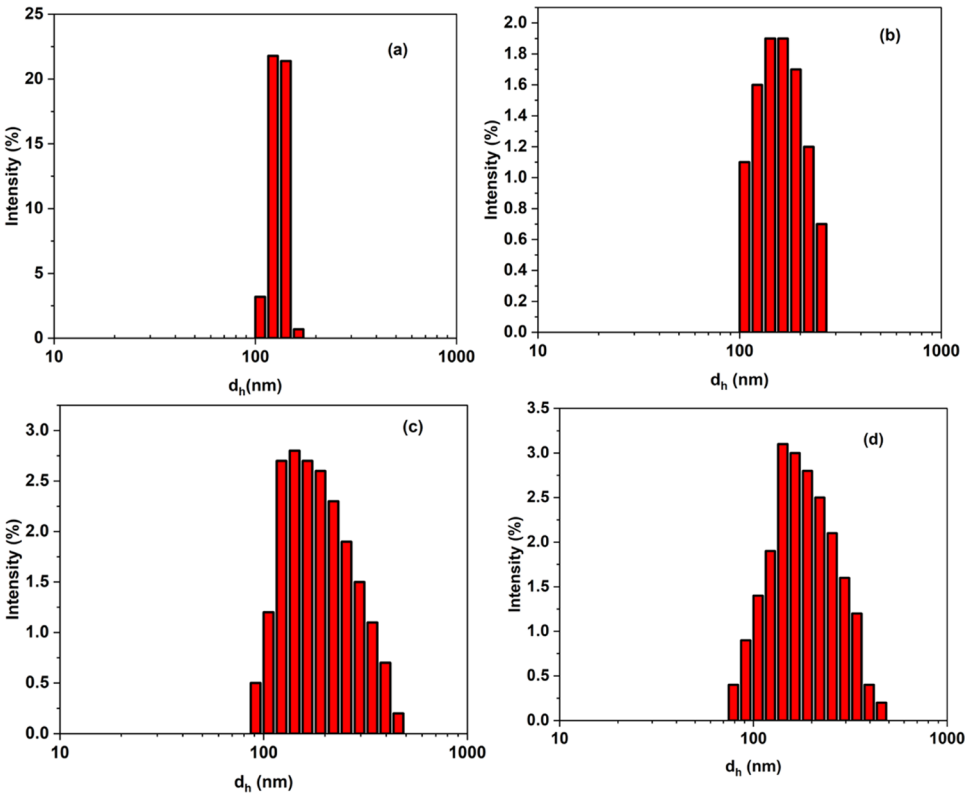

Figure 4. Histograms showing the hydrodynamic size distributions of (a) SLN1, (b) CUR-SLN1, (c) CUR-SLN2, and (d) CUR-SLN3 in aqueous suspension.

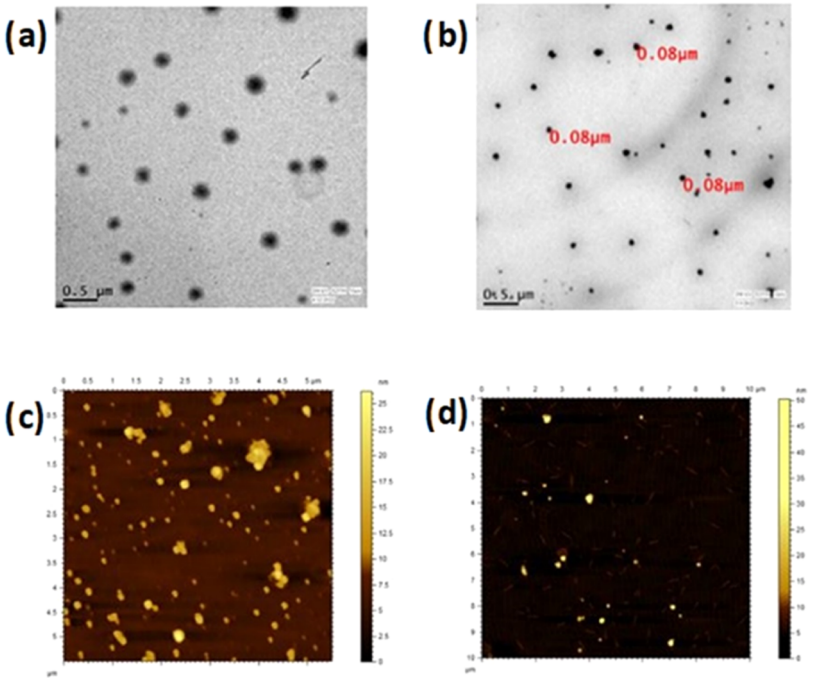

Figure 5. Upper panel: unstained TEM images of (a) blank SLN and (b) CUR-SLN3. Lower panel: AFM images of (c) blank SLN and (d) CUR-SLN3.

Stability Studies. Often physical (aggregation) and chemical instability phenomena are observed to appear when SLNs are formulated as aqueous suspensions, which limits their applications. Usually, lyophilization is used to overcome the physical instability of SLN suspensions.[43] To evaluate the ability of the prepared formulation to retain its physical and chemical characteristics, we performed stability studies, which recommend the storage conditions to maintain the quality, safety, and efficacy throughout the storage period of the developed formulation. The particle size and PDI are important factors

https://doi.org/10.1021/acsabm.3c00252
ACS Appl. Bio Mater. 2023, 6, 2785−2794

in judging the physical stability of nanocarriers. According to data in Tables 1 and 2, the PDI of blank SLN1 is low, suggesting higher physical stability of the suspension. The ZP that indicates the surface charge density on the suspended SLNs in water is also an important parameter for the determination of the physical stability of the SLN suspension. A higher value of ZP (positive or negative) suggests stability of the dispersion because a higher charge resists aggregation. The higher negative value of ZP (−29 mV) of the blank SLN1, as well as CUR-SLN suspensions, suggests its sufficient stability. The negative ζ potential of the SLN must be related to the partially ionized free −COOH groups at the lipid head.

The stability of blank SLN1 at higher temperatures was also investigated by turbidity (τ = 100 − %T, where T is the transmittance) measurements. The transmittance of the dilute SLN1 suspension was recorded at different temperatures in the range of 25−70 °C. The plot of τ vs T (°C) is shown in Figure 6,

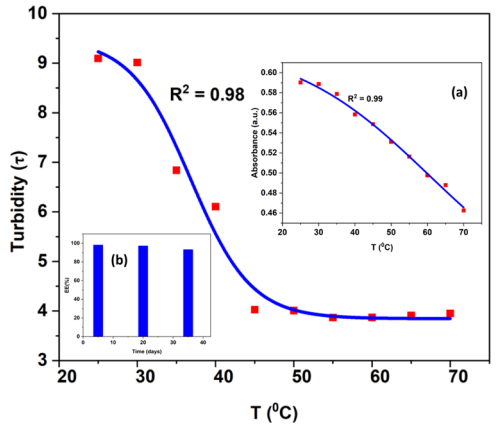

Figure 6. Plot of turbidity of the SLN1 dispersion versus temperature; insets: (a) degradation of CUR-SLN3 with temperature and (b) variation of EE (%) of CUR-SLN3 with time.

which shows a small decrease in turbidity with an increase in temperature. This is due to the increase of the aqueous solubility of lipids at higher temperatures, which leads to the dissolution of nanoparticles in water. However, the SLN dispersion is quite stable at the physiological temperature (37 °C).

Also, it can be found from the data presented in Table 2 that the PDI value of the SLN1 suspension is observed to increase on the incorporation of CUR, indicating the relatively lower stability of the suspension. In the present work, the nanoformulations were evaluated for mean %EE (stored at 4 °C). The prepared aqueous suspension of SLN was stored in a closed container at 4 °C and at room temperature (~30 °C) for 3 months. The results are presented in Figure 6b (inset). Due to the lipophilic nature of CUR, up to 98% EE was achieved, which decreased to 93% after 35 days. As also reported by others, this may be due to polymorphic transitions of the lipid matrices with subsequent drug expulsion.[44] This is indicated by the increase in the PDI value on storage. Indeed, the movement of lipid chains causes the diffusion of drug molecules from the SLN matrix. This means that there is a loss of EE due to drug leaching during storage.

It is also essential to test the chemical stability of encapsulated drugs as it provides an indication of the variation in the quality of the pharmaceutically active agent under the influence of environmental conditions. Therefore, the thermal stability of encapsulated CUR was studied in the temperature range of 25−70 °C through the measurement of UV−vis absorption spectra. The results are presented in Figure 6a (inset). It is observed that the absorbance value for entrapped CUR gradually decreases with an increase in temperature, suggesting slow thermal degradation of CUR. This means that the lipid matrix protects CUR from thermal degradation. Also, we measured the UV−vis spectrum of the CUR-SLN3 suspension and compared it with the spectrum of free CUR in PBS after 48 h. The spectrum of CUR-SLN3 resembled that of the freshly prepared CUR-SLN suspension in water even after 3 months (Figure 2a). The corresponding fluorescence spectrum (Figure 2b) also looks similar to that of a freshly prepared sample, suggesting good storage stability of entrapped CUR. In contrast, the free CUR spectrum exhibits a large change from the freshly prepared sample, indicating its rapid degradation in PBS at room temperature. These results show the significant protection ability of the developed SLN from aqueous degradation of CUR.

In Vitro Drug Release Kinetics. The in vitro release study was performed at 37 °C in a release medium (PBS, pH 7.4) containing 2.5% T80, and the leaching of CUR was monitored for 38 h. The release profiles of CUR-SLN3 and CUR-SLN4 are depicted in Figure 7. As observed, there is no significant release

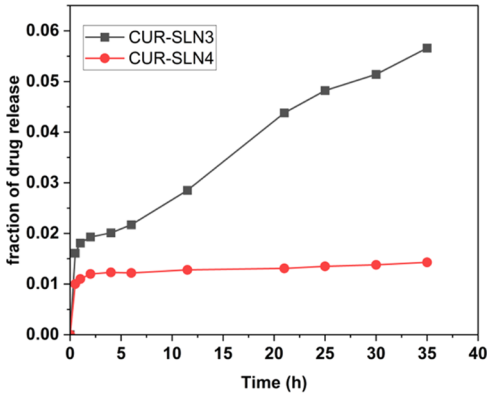

Figure 7. In vitro drug release profiles of CUR-SLN3 and CUR-SLN4 in PBS containing 2.5% T80, pH 7.4 at 37 °C.

of CUR in the case of CUR-SLN4. However, the maximum attainable CUR release after 38 h in the case of CUR-SLN3 is ~6%. At 37 °C, the SLNs are in the solid state and the mobility of entrapped CUR molecules reduces, resulting in slow release. The relatively low amount of CUR release indicates that the nanoformulation is very stable with long shelf life, which suggests that the SLN formulation can be used for sustained release of CUR. For both CUR-SLN3 and CUR-SLN4, there is a burst release followed by a slow release of CUR. The release profiles, however, could not be fitted to any standard equations[45] proposed for in vitro drug release. The initial burst release can be attributed to the desorption of CUR from the surface of the SLN. This is followed by a slow release, which is due to the diffusion of CUR through the lipid matrix. The higher rate of drug release in the case of CUR-SLN3 can be attributed to the −OH group in the fatty acid chain that allows water molecules to penetrate easily into the pores of the matrix, leading to greater CUR release with respect to CUR-SLN4 particles consisting of C_{14}-GABA. A similar effect of hydroxyl groups has also been reported in the literature.[46]

In Vitro Cytotoxicity Studies. CUR-SLN-induced cytotoxicity in both human breast cancer MCF7 and prostate cancer PC3 cell lines was investigated by the MTT assay in the presence

https://doi.org/10.1021/acsabm.3c00252
ACS Appl. Bio Mater. 2023, 6, 2785−2794

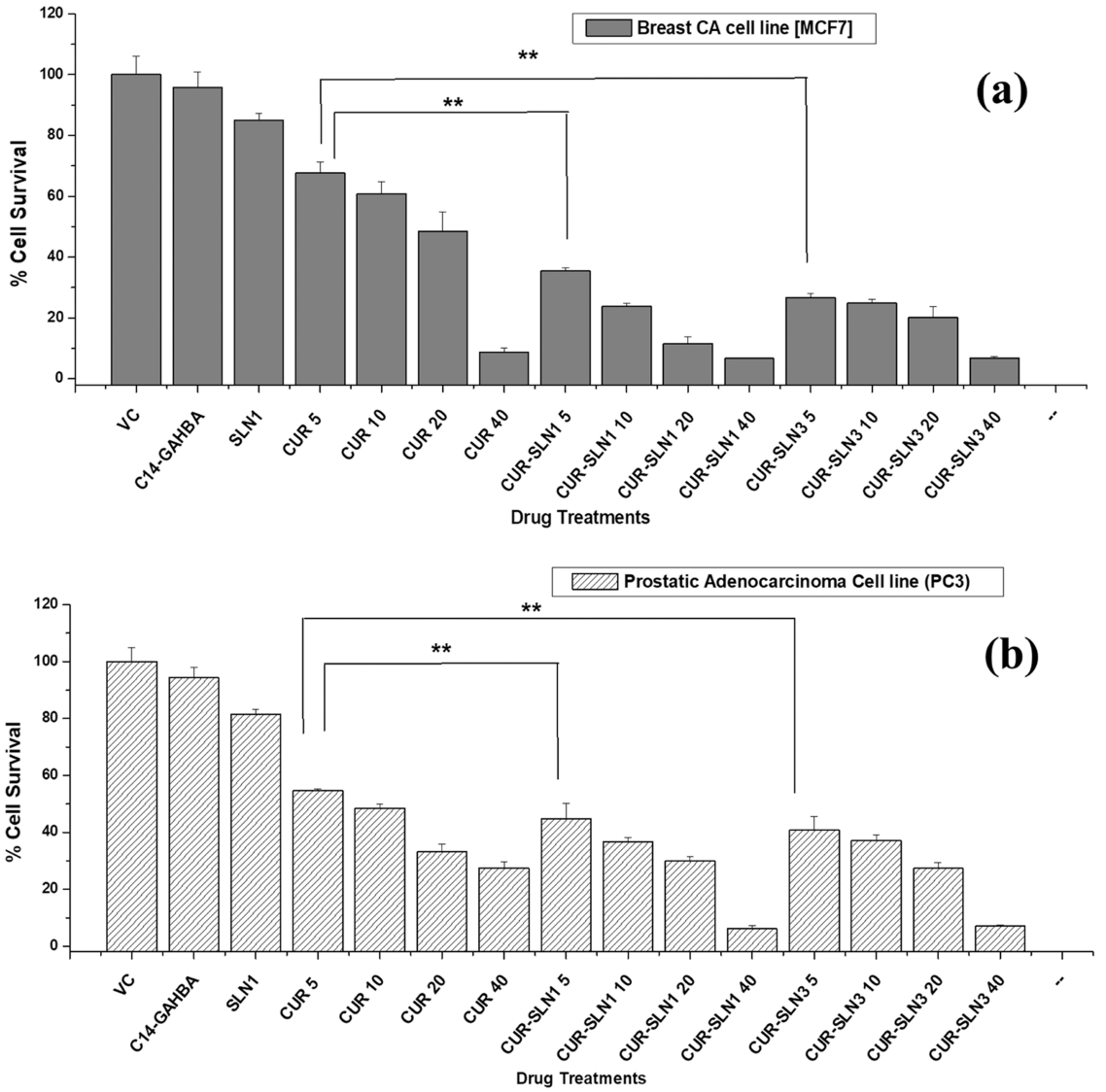

Figure 8. Lipid, CUR, blank SLN1, and CUR-SLN induced cytotoxicity in (a) MCF7 and (b) PC3 cells; results presented are the mean of SD ($n = 3$) (**$P < 0.001$) when compared between CUR-only and CUR-SLN groups.

of varying concentrations of CUR and their corresponding SLN formulations keeping vehicle control and unloaded SLN1 as references. Also, we performed the MTT assay for the pure C_{14}-GAHBA lipid. The cell lines were treated for 24 h with different concentrations of CUR-SLN preparations along with the vehicle control. The percent cell viability at various concentrations of lipid, CUR, and CUR-SLN are presented in Figure 8. It is observed that neither pure lipid nor the blank SLN1 has any significant cytotoxicity. However, as shown in Figure 8a, CUR induces cell death in a concentration-dependent manner in the human breast cancer MCF7 cell line. The cytotoxicity is further enhanced by ∼25.4 and 34.1% with 5 μM CUR-SLN1 and CUR-SLN3, respectively. The enhancement of cytotoxicity is persistent with a higher concentration of CUR-loaded SLN1 as well. The SLN1 alone, however, shows minimal cytotoxicity at the working concentration of 5−40 μg/mL. As presented in Figure 8b, a similar trend is also observed in prostate cancer cell line PC3 with a significant increase in cytotoxicity in CUR-loaded SLN groups ($P < 0.001$). Relevantly, different SLNs alone show very low cytotoxicity pertaining to the earlier reports. Thus, the synthesized lipid molecule and the SLNs prepared from it are biocompatible.

CONCLUSIONS

In this work, a stable SLN formulation of CUR was prepared using a semisynthetic lipid. The −OH group at the lipid head was found to enhance the physical stability of the SLN formulation. An entrapment efficiency of CUR close to its solubility in the molten lipid was achieved. The results suggested that the lipid matrix protects CUR from thermal and environmental degradation in aqueous dispersions. Although the synthesized lipid molecule and the SLNs prepared from it are biocompatible, the MTT-based cytotoxicity assay shows that an SLN1-encapsulated CUR delivery system significantly reduces the proliferation/viability of human breast cancer MCF7 cells and human prostatic adenocarcinoma PC3 cells in a dose-dependent manner. This study indicates that CUR-SLNs could be a potential chemotherapeutic formulation for breast cancer therapy.

https://doi.org/10.1021/acsabm.3c00252
ACS Appl. Bio Mater. 2023, 6, 2785−2794

■ ASSOCIATED CONTENT

Supporting Information

The Supporting Information is available free of charge at https://pubs.acs.org/doi/10.1021/acsabm.3c00252.

Details of the synthetic procedure; chemical identification data; FTIR, ^{1}H NMR, ^{13}C NMR, and HRMS spectra (Figures S1−S5) (PDF)

■ AUTHOR INFORMATION

Corresponding Author

Joykrishna Dey − *Department of Chemistry, Indian Institute of Technology Kharagpur, Kharagpur 721302, India;* orcid.org/0000-0001-8357-5560; Email: joydey@chem.iitkgp.ac.in

Authors

Swagata Patra − *Department of Chemistry, Indian Institute of Technology Kharagpur, Kharagpur 721302, India*

Avik Chakraborty − *Radiation Medicine Centre, Bhabha Atomic Research Centre, Parel, Mumbai 400012, India*

Complete contact information is available at: https://pubs.acs.org/10.1021/acsabm.3c00252

Notes

The authors declare no competing financial interest.

■ ACKNOWLEDGMENTS

The authors acknowledge the Ministry of Education, Government of India and the Indian Institute of Technology Kharagpur for providing financial support and infrastructure, respectively. The authors also thank Mr. Somnath Kar (Radiation Medicine Centre, BARC, India) for his help with the biochemical assays and Dr. N. Sarkar (IIT Kharagpur) for assistance with the DLS measurements.

■ REFERENCES

(1) Gupta, T.; Singh, J.; Kaur, S.; Sandhu, S.; Singh, G.; Kaur, I. P. Enhancing Bioavailability and Stability of Curcumin Using Solid Lipid Nanoparticles (CLEN): A Covenant for Its Effectiveness. *Front. Bioeng. Biotechnol* **2020**, *8*, No. 879.

(2) Abd-Ellatef, G.-E. F.; Gazzano, E.; Chirio, D.; Hamed, A. R.; Belisario, D. C.; Zuddas, C.; Peira, E.; Rolando, B.; Kopecka, J.; Marie, M. A. S.; Sapino, S.; Fahmy, S. R.; Gallarate, M.; Hamid, A. H. Z.; Riganti, C. Curcumin-Loaded Solid Lipid Nanoparticles Bypass P-Glycoprotein Mediated Doxorubicin Resistance in Triple Negative Breast Cancer Cells. *Pharmaceutics* **2020**, *12*, No. 96.

(3) Anand, P.; Sundaram, C.; Jhurani, S.; Kunnumakkara, A. B.; Aggarwal, B. B. Curcumin and cancer: an "old-age" disease with an "age-old" solution. *Cancer Lett.* **2008**, *267*, 133−164.

(4) Bachmeier, B.; Nerlich, A. G.; Iancu, C. M.; Cilli, M.; Schleicher, E.; Vene, R.; Dell'Eva, R.; Jochum, M.; Albini, A.; Pfeffer, U. The chemopreventive polyphenol curcumin prevents hematogenous breast cancer metastases in immunodeficient mice. *Cell Physiol. Biochem.* **2007**, *19*, 137−152.

(5) Goel, A.; Kunnumakkara, A. B.; Aggarwal, B. B. Curcumin as "curecumin": from kitchen to clinic. *Biochem. Pharmacol.* **2008**, *75*, 787−809.

(6) Yoysungnoen, P.; Wirachwong, P.; Bhattarakosol, P.; Niimi, H.; Patumraj, S. Effects of curcumin on tumor angiogenesis and biomarkers, COX-2 and VEGF, in hepatocellular carcinoma cellimplanted nude mice. *Clin. Hemorheol. Microcirc.* **2006**, *234*, 109−115.

(7) Mukerjee, A.; Vishwanatha, J. K. Formulation, characterization and evaluation of curcumin-loaded PLGA nanospheres for cancer therapy. *Anti-Cancer Res.* **2009**, *29*, 3867−3875.

(8) Gou, M.; Men, K.; Shi, H.; Xiang, M.; Zhang, J.; Song, J.; Long, J.; Wan, Y.; Luo, F.; Zhao, X.; Qian, Z. Curcumin-loaded biodegradable polymeric micelles for colon cancer therapy in vitro and in vivo. *Nanoscale* **2011**, *3*, 1558−1567.

(9) Li, L.; Braiteh, F. S.; Kurzrock, R. Liposome-encapsulated curcumin: in vitro and in vivo effects on proliferation, apoptosis, signaling, and angiogenesis. *Cancer* **2005**, *104*, 1322−1331.

(10) Tagne, J. B.; Kakumanu, S.; Nicolosi, R. J. Nano-emulsion Preparations of the Anti-cancer Drug Dacarbazine Significantly Increase Its Efficacy in a Xenograft Mouse Melanoma Model. *Mol. Pharmaceutics* **2008**, *5*, 1055−1063.

(11) Zhang, Q.; Colazo, J.; Berg, D.; Mugo, S. M.; Serpe, M. J. Multiresponsive Nanogels for Targeted Anti-cancer Drug Delivery. *Mol. Pharmaceutics* **2017**, *14*, 2624−2628.

(12) Mehnert, W.; Mäder, K. Solid lipid nanoparticles: production, characterization and applications. *Adv. Drug Delivery Rev.* **2001**, *47*, 165−196.

(13) Tang, H.; Murphy, C. J.; Zhang, B.; Shen, Y.; Kirk, E. A. V.; Murdoch, W. J.; Radosz, M. Curcumin polymers as anti-cancer conjugates. *Biomaterials* **2010**, *31*, 7139−7149.

(14) Wang, W.; Chen, T.; Xu, H.; Ren, B.; Cheng, X.; Qi, R.; Liu, H.; Wang, Y.; Yan, L.; Chen, S.; Yang, Q.; Chen, C. Curcumin-Loaded Solid Lipid Nanoparticles Enhanced Anti-cancer Efficiency in Breast Cancer. *Molecules* **2018**, *23*, 1578.

(15) Duan, Y.; Dhar, A.; Patel, C.; Khimani, M.; Neogi, S.; Sharma, P.; Nadavala, S. K.; Vekariya, R. L. A brief review on solid lipid nanoparticles: part and parcel of contemporary drug delivery systems. *RSC Adv.* **2020**, *10*, 26777−26791.

(16) Karimitabar, Z.; Chegini, Z.; Shokoohizadeh, L.; Moez, N. M.; Arabestani, M. R.; Hosseini, S. M. Use of the quantum dot-labeled solid lipid nanoparticles for delivery of streptomycin and hydroxychloroquine: A new therapeutic approach for the treatment of intracellular Brucella abortus infection. *Biomed Pharmacother.* **2023**, *158*, No. 114116.

(17) De, A.; Roychowdhury, P.; Bhuyan, N. R.; Ko, Y. T.; Singh, S. K.; Dua, K.; Kuppusamy, G. Folic Acid Functionalized Diallyl Trisulfide−Solid Lipid Nanoparticles for Targeting Triple Negative Breast Cancer. *Molecules* **2023**, *28*, 1393.

(18) Taniyadukkam, V.; Jose, J.; Maliyakkal, N.; Beeran, A. A.; Almoyad, M. A. A.; Aleya, L.; Bandiwadekar, A. Development and evaluation of sunscreen cream containing solid lipid nanoparticles of Spinacia oleraceae. *Environ. Sci. Pollut. Res.* **2023**, *30*, 51782−51791.

(19) Sommonte, F.; Arduino, I.; Iacobazzi, R. M.; Tiboni, M.; Catalano, F.; Marotta, R.; Francesco, M. D.; Casettari, L.; Decuzzi, P.; Lopedota, A. A.; Denora, N. Microfluidic assembly of "Turtle-Like" shaped solid lipid nanoparticles for lysozyme delivery. *Int. J. Pharm.* **2023**, *631*, No. 122479.

(20) Aanisah, N.; Sulistiawati, S.; Djabir, Y. Y.; Asri, R. M.; Sumarheni, S.; Chabib, L.; Hamzah, H.; Permana, A. D. Development of Solid Lipid Nanoparticle-Loaded Polymeric Hydrogels Containing Antioxidant and Photoprotective Bioactive Compounds of Safflower (*Carthamus tinctorius* L.) for Improved Skin Delivery. *Langmuir* **2023**, *39*, 1838−1851.

(21) Rosa, A.; Nieddu, M.; Pitzanti, G.; Pireddu, R.; Lai, F.; Cristina, M. Impact of solid lipid nanoparticles on 3T3 fibroblasts viability and lipid profile: The effect of curcumin and resveratrol loading. *J Appl Toxicol.* **2023**, *43*, 272−286.

(22) Badawi, N.; Say, K. E.; Attia, D.; Nabarawi, M.; Elmazar, M.; Teaima, M. Development of Pomegranate Extract-Loaded Solid Lipid Nanoparticles: Quality by Design Approach to Screen the Variables Affecting the Quality Attributes and Characterization. *ACS Omega* **2020**, *5*, 21712−21721.

(23) Sadegh Malvajerd, S.; Azadi, A.; Izadi, Z.; Kurd, M.; Dara, T.; Dibaei, M.; Zadeh, M. S.; Javar, H. A.; Hamidi, M. Brain Delivery of Curcumin Using Solid Lipid Nanoparticles and Nanostructured Lipid

Carriers: Preparation, Optimization, and Pharmacokinetic Evaluation. *ACS Chem. Neurosci.* **2019**, *10*, 728−739.
(24) Elbrink, K.; Hees, S. V.; Chamanza, R.; Roelant, D.; Loomans, T.; Holm, R.; Kiekens, F. Application of solid lipid nanoparticles as a long-term drug delivery platform for intramuscular and subcutaneous administration: In vitro and in vivo evaluation. *Eur. J. Pharm. Biopharm.* **2021**, *163*, 158−170.
(25) Scioli Montoto, S.; Sbaraglini, M. L.; Alevi, A.; Couyoupetroub, M.; Ianni, M. D.; Pesce, G. O.; Alvarezc, V. A.; Bruno-Blancha, L. E.; Castro, G. R.; Ruiz, M. E.; Islan, G. A. Carbamazepine-loaded solid lipid nanoparticles and nanostructuredlipid carriers: Physicochemical characterization and in vitro/in vivo evaluation. *Colloids Surf., B* **2018**, *167*, 73−81.
(26) Demirbilek, M.; Turkoglu, N. L.; Akturk, S.; Akca, C. VitD3-loaded solid lipid nanoparticles: stability, cytotoxicity and cytokine levels. *J. Microencpsul.* **2017**, *34*, 454−462.
(27) Garg, N. K.; Singh, B.; Jain, A.; Nirbhavane, P.; Sharma, R.; Tyagi, R. K.; Kushwah, V.; Jain, S.; Katare, O. P. Fucose decorated solid-lipid nanocarriers mediate efficient delivery of methotrexate in breast cancer therapeutics. *Colloids Surf., B* **2016**, *146*, 114−126.
(28) Nemati, E.; Mokhtarzadeh, A.; Azar, V. P.; Mohammadi, A.; Hamishehkar, H.; Abbasi, M. M.; Dolatabadi, J. E. N.; Guardia, M. Ethambutol-Loaded Solid Lipid Nanoparticles as Dry Powder Inhalable Formulation for Tuberculosis Therapy. *AAPS PharmSciTech* **2019**, *20*, No. 120.
(29) Chantaburanan, T.; Teeranachaideekul, V.; Chantasart, D.; Jintapattanakit, A.; Junyaprasert, V. B. Effect of binary solid lipid matrix of wax and triglyceride on lipid crystallinity, drug-lipid interaction and drug release of ibuprofen-loaded solid lipid nanoparticles (SLN) for dermal delivery. *J. Colloid Interface Sci.* **2017**, *504*, 247−256.
(30) Ganesan, P.; Narayanasamy, D. Lipid nanoparticles: different preparation techniques, characterization, hurdles, and strategies for the production of solid lipid nanoparticles and nanostructured lipid carriers for oral drug delivery. *Sustainable Chem. Pharm.* **2017**, *6*, 37−56.
(31) Morales, T. I.; Stearns-Yoder, K. A.; Hoffberg, A. S.; Khan, T. K.; Wortzel, H.; Brenner, L. A. Interactions of Glutamate and Gamma Amino Butyric Acid with the insulin-like growth factor system in traumatic brain injury (TBI) and/or cardiovascular accidents (CVA or stroke): A systematic review. *Heliyon* **2022**, *8*, No. e09037.
(32) Wang, L.; Liu, Y.; Yu, Z.; Gong, J.; Deng, Z.; Ren, N.; Zhong, Z.; Cai, H.; Tang, Z.; Cheng, H.; Chen, S.; He, Z. Mir-139-5p inhibits glioma cell proliferation and progression by targeting GABRA1. *J. Transl. Med.* **2021**, *19*, 213.
(33) Bown, A. W.; Shelp, B. J. The Metabolism and functions of γ-aminobutyric Acid. *Plant Physiol.* **1997**, *115*, 1−5.
(34) Baxter, C. F.; Lajtha, A. The nature of γ-aminobutyric Acid. In *Handbook of Neurochemistry. Volume III: Metabolic Reactions in the Nervous System*. Ed.; Plenum Press: New York, 1970, *Chapter 9*, 289−353.
(35) Arora, R.; Katiyar, S. S.; Kushwah, V.; Jain, S. Solid lipid nanoparticles and nanostructured lipid carrier-based nanotherapeutics in treatment of psoriasis: a comparative study. *Expert Opin. Drug Delivery* **2017**, *14*, 165−177.
(36) Pandey, V.; Haider, T.; Chandak, A. R.; Chakraborty, A.; Banerjee, S.; Soni, V. Surface modified silk fibroin nanoparticles for improved delivery of doxorubicin: Development, characterization, in-vitro studies. *Int. J. Biol. Macromol.* **2020**, *164*, 2018−2027.
(37) Lopes, R.; Eleutério, C.; Gonçalves, L.; Cruz, M.; Almedia, A. Lipid nanoparticles containing orizalin for the treatment of leishmaniasis. *Eur. J. Pharm. Sci.* **2012**, *45*, 442−450.
(38) Chirio, D.; Peira, E.; Dianzani, C.; Muntoni, E.; Gigliotti, C. L.; Ferrara, B.; Sapino, S.; Chindamo, G.; Gallarate, M. Development of solid lipid nanoparticles by cold dilution of microemulsions: Curcumin loading, preliminary in vitro studies, and biodistribution. *Nanomaterials* **2019**, *9*, 230−246.
(39) Mehnert, W.; Mäder, K. Solid lipid nanoparticles production, characterization, and applications. *Adv. Drug Delivery Rev.* **2012**, *64*, 83−101.
(40) Lackowicz, J. R. Principles of Fluorescence Spectroscopy 3rd ed.; USA, 2008.
(41) Banerjee, C.; Maiti, S.; Mustafi, M.; Kuchlyan, J.; Banik, D.; Kundu, N.; Dhara, D.; Sarkar, N. Effect of encapsulation of curcumin in polymeric nanoparticles: how efficient to control ESIPT process? *Langmuir* **2014**, *30*, 10834−10844.
(42) Siekmann, B.; Wesesen, K. Melt-homogenized solid lipid nanoparticles stabilized by the non-ionic surfactant tylxapol. I. Preparation and particle size determination. *Pharm. Pharmacol. Lett.* **1994**, *3*, 194−197.
(43) Banerjee, I.; De, K.; Mukherjee, D.; Dey, G.; Chattopadhyay, S.; Mukherjee, M.; Mandal, M.; Bandyopadhyay, A. K.; Gupta, A.; Ganguly, S.; Mishra, M. Paclitaxel-loaded solid lipid nanoparticles modified with Tyr-3-octreotide for enhanced anti-angiogenic and anti-glioma therapy. *Acta Biomater.* **2016**, *38*, 69−81.
(44) Wissing, S.; Kayser, O.; Müller, R. Solid lipid nanoparticles for parenteral drug delivery. *Adv. Drug Delivery Rev.* **2004**, *56*, 1257−1272.
(45) Aydin, R.; Pulat, M. 5-Fluorouracil encapsulated chitosan nanoparticles for pH-stimulated drug delivery: evaluation of controlled release kinetics. *J. Nanomater.* **2012**, *42*, No. 313961.
(46) Kheradmandnia, S.; Vasheghani-Farahani, E.; Nosrati, M.; Atyabi, F. Preparation and characterization of ketoprofen-loaded solid lipid nanoparticles made from beeswax and carnauba wax. *Nanomed.: Nanotechnol. Biol. Med.* **2010**, *6*, 753−759.

https://doi.org/10.1021/acsabm.3c00252
ACS Appl. Bio Mater. 2023, 6, 2785−2794